

Innovative Organic Electroluminescent Materials with a Doublet Ground State: A Theoretical Investigation

Huixue Li,* Xiaofeng Wang, Yuancheng Zhu, and Zhifeng Li*

Cite This: *J. Phys. Chem. A* 2020, 124, 662–673

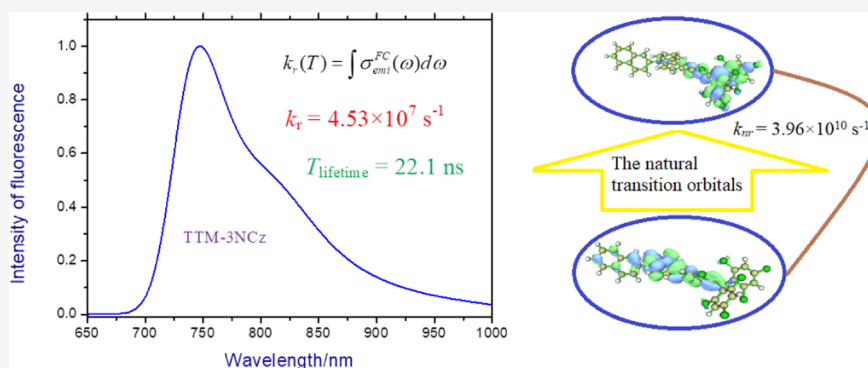
Read Online

ACCESS |

Metrics & More

Article Recommendations

Supporting Information



ABSTRACT: The displaced and distorted harmonic oscillator model, which has been proven to be appropriate in calculating vibronic spectra, is employed to treat the emission spectrum of title molecules in combination with a thermal vibration correlation function. The calculated results indicate that the main peak of the emission spectrum is visibly impacted by the normal modes with lower frequencies and that the shoulder peak is originated from the middle-frequency modes. On the level of time-dependent density functional theory (TDDFT), the calculated fluorescence lifetimes of TTM-3NCz and TTM-3PCz are 22.1 and 26.0 ns, respectively, which happen to coincide with the observed values of TTM-3NCz (17.2 ns) and TTM-3PCz (21.2 ns). The above data indicate that both the calculated radiative decay rates are reasonable at room temperature. Furthermore, we investigate the influence of the Duschinsky effect on the fluorescence quantum efficiency (FQE). When it is considered, the predicted FQE of the TTM-3NCz molecule is only 0.11%, and the observed value (49% in toluene) deviates significantly. If we ignore the Duschinsky effect, the FQE of TTM-3NCz increases dramatically to 41.8%. For the TTM-3PCz molecule (the FQE is 46% in toluene), the calculated FQE is 0.042% with the Duschinsky effect and increases to 45.2% without the Duschinsky effect. This phenomenon might be related to external factors and the nature of the TDDFT only considering a single configuration. In addition, the fluorescent properties of the fluorinated TTM-3NCz molecules are studied predictably. The obtained results show that the perfluorinated TTM-3NCz shows better luminous performance due to larger oscillator strength. Finally, the dimers, which are composed of both single title molecules, are explored theoretically to determine how they impact the fluorescent property; however, the effect can be nearly eliminated because of the small binding energies.

1. INTRODUCTION

With the rapid development of all sorts of light-emitting materials used in organic light-emitting diodes (OLEDs), the device has achieved significant progress and attracted great attention from the industry and academy. The outstanding performances of OLED, such as wide viewing angle, low power consumption, flexible structure, and abundant species, ensure that the device has an overwhelming advantage in the display field.^{1–5} However, the vast majority of the existing electroluminescent materials are closed-shell systems, since the singlet excited state can only be allowed to radiatively decay and the electron transition between the triplet state and the ground state is spin-forbidden, which implies that the maximum value of the internal quantum efficiency (IQE) is only 25% based on the quantum spin statistics.⁶ In view of this situation, there are

many ways having been developed to improve IQE. The exploitation of the phosphorescent materials is a good choice and has achieved great success. IQE can reach up to almost 100% by utilizing both singlet and triplet excitons.^{7,8} Thermally activated fluorescent materials can also harvest the triplet exciton and increase IQE. This strategy turns triplets into singlets by reverse intersystem crossing with the aid of the environment thermal energy, which improves the energy utilization rate. Another key benefit of the materials is that the

Received: November 4, 2019

Revised: December 25, 2019

Published: January 7, 2020

use of expensive noble metal-based phosphorescent materials can be avoided.^{5,9,10} Triplet–triplet annihilation (TTA) is an additional feasible method, wherein two triplets annihilate each other. Meanwhile, one singlet can be generated, and 62.5% of the up-limit IQE can be achieved in this process.^{11,12} Recently, Li et al. synthesized a new kind of electroluminescent material as an emitter, which possesses electrically neutral π -radicals and is a doublet state. Due to the spin-allowed transition from the excited doublet state to the ground state, the IQE can reach 100% theoretically.^{13–15} They found that the experimental IQE of the novel luminescent material TTM-3NCz in the solid state, which was synthesized by incorporating (naphthalen-2-yl)-9H-carbazole (3NCz) into the tris(2,4,6-trichlorophenyl)methyl (TTM) radical, is near 91% and that of the other emitter TTM-3PCz (phenyl-9H-carbazole) is 61%. The maximum external quantum efficiencies of the OLEDs, in which TTM-3NCz and TTM-3PCz act as deep red electroluminescent materials, are 26.5 and 16.6%, respectively. This implied that the IQEs of both compounds reach near 100% in the OLED. In addition, a theoretical discussion was carried out in combination with the molecular orbital diagrams of the geometry-optimized TTM and TTM-3NCz structures. They depicted the mechanism of the electron transition process. These calculated results gave a better understanding of excited-state processes. Nevertheless, the details of excited-state processes involved radiative and nonradiative decay rates remain unknown, it is necessary to discuss the underlying mechanism further.

Generally, the frontier molecular orbitals can observe visually the process of electron transition between the ground state and the excited states, which is helpful to reveal the luminescence mechanism; however, the fluorescent efficiency relies on the competition between the radiative rate and the nonradiative rate; thus, both the rates must primarily be acquired. Shuai et al. contributed a method to theoretically treat the fluorescent quantum efficiency of a polyatomic molecule in optoelectronic devices,¹⁶ which can quantitatively calculate the radiative and nonradiative decay rates by combining with the harmonic oscillator model. Then, the IQE of fluorescent materials can be determined further. In this paper, we have employed density functional theory (DFT) and time-dependent DFT (TDDFT) to study spectroscopic properties and excited-state geometric and electronic structures of both the compounds. In addition, we calculated corresponding radiative and nonradiative rates in combination with a thermal vibration correlation function. Furthermore, the influence of the Duschinsky effect on the fluorescence quantum efficiency was investigated, and at the same time, the photochemical reaction was ignored. If this is the main process, the performance of OLED would degrade at once.¹⁷ To obtain better fluorescent materials, the fluorinated TTM-3NCz molecule was predictively studied. Moreover, the effect on the fluorescence of the dimers composed of both the single title molecules was explored too.

2. THEORETICAL METHOD AND COMPUTATIONAL DETAILS

2.1. Theoretical Method. The radiative decay rate can be computed by the Einstein spontaneous emission rate and Fermi gold rule, which can be expressed by the integration over the whole emission spectrum^{16,18}

$$k_r(T) = \int \sigma_{\text{emi}}^{\text{FC}}(\omega) d\omega \quad (1)$$

where $\sigma_{\text{emi}}^{\text{FC}}$ is the emission cross section with dimensions in square centimeters. The explicit expression is given by the following formula

$$\sigma_{\text{emi}}(\omega) = \frac{4\omega^3}{3hc^3} \sum_{v_i, v_f} P_{v_i}(T) |\langle \theta_{f,v_f} | \mu_{fi} | \theta_{i,v_i} \rangle|^2 \delta(\omega_{iv_f} - \omega) \quad (2)$$

Here, c is the velocity of light, $P_{v_i}(T)$ is the Boltzmann population of initial states, and μ_{fi} is the electric transition dipole moment. For the strongly dipole-allowed transitions of the molecules, only the zeroth-order term is taken into account; thus, the electron transition dipole moment can be simplified to $\mu_{fi} = \langle \phi_i | \mu_0 | \phi_f \rangle$, and ϕ and θ are the electronic and vibrational wave functions, respectively. The delta function in eq 2 by the Fourier transformation, the above formula can be eventually expressed an analytical integral formalism

$$\sigma_{\text{emi}}^{\text{FC}}(\omega) = \frac{4\omega^3}{3hc^3} |\mu_0|^2 \int_{-\infty}^{\infty} e^{-i(\omega - \omega_{if})t} Z_{iv}^{-1} \rho_{\text{em},0}^{\text{FC}}(t, T) dt \quad (3)$$

Here, Z_{iv} is the partition function and $\rho_{\text{em},0}^{\text{FC}}$ is the correlation function of time and temperature, which are calculated by the multidimensional harmonic oscillator model using the MOMAP package.¹⁹ Similar to the spontaneous emission, the nonradiative internal conversion (IC) processes can be dealt with Fermi's golden rule by the displaced harmonic oscillator model, and the IC rate can be expressed as^{16,18}

$$k_{\text{IC}} = \sum_{kl} k_{ic,kl} \quad (4)$$

$$k_{ic,kl} = \frac{1}{h^2} R_{kl} \int_{-\infty}^{\infty} dt [e^{-i\omega_{if}t} Z_{iv}^{-1} \rho_{ic,kl}(t, T)] \quad (5)$$

where R_{kl} is the nonadiabatic transition momentum containing both diagonal and nondiagonal terms, Z_{iv} is the partition function, and $\rho_{ic,kl}$ is the thermal vibrational correlation function in the internal conversion process, which was expounded detailedly in the Supporting Information (see the Section 2.1). Intersystem crossing may occur between different states, however, if the conical intersection is involved, of which the decay rate is usually greater than 10^{12} s^{-1} ;^{16,20} luckily, our work showed that all of the calculated radiative decay rates (k_r) and nonradiative decay rates (k_{nr}) were less than 10^{12} s^{-1} . Thus, the influence of the intersystem crossing can be omitted. We employed the MOMAP package to acquire the fluorescent spectra and rate constants of the title molecules. Further, the other fluorescent parameters can be investigated theoretically.¹⁹

When photochemistry and the intersystem crossing were not taken into account, the molecular light-emitting efficiency is determined by the competition between the radiative decay rate (k_r) and the nonradiative decay rate (k_{nr}); here, k_{nr} is only the internal conversion rate. The fluorescence quantum yield can be expressed as $\eta = k_r / (k_r + k_{\text{nr}})$. According to this formula, either suppressing the nonradiative rate or increasing the radiative rate can promote higher fluorescence efficiency.

2.2. Computational Details. The geometry optimization of the TTM-3NCz and TTM-3PCz molecules was implemented with the Gaussian 09 program package.²¹ The geometries of the ground states (S_0) were optimized using

the UB3LYP/6-31+(d) level; for the low-lying doublet excited electronic state (S_1), the TD-UB3LYP approach was employed with the same basis set. Harmonic vibrational frequencies of these optimized minima were calculated, and no virtual frequency was found, which confirmed the stability of the equilibrium geometries of the S_0 and S_1 states. In general, due to the nature of the single-excited configuration, TDDFT has inherent limitation in describing the highly excited state with the common exchange correlation functional. It is only appropriate for the low-lying excited state.²² Fortunately, one can see in the discussion section the S_1 state of TTM-3NCz and TTM-3PCz molecules, which were related to electron transition characteristics, mainly originating from the HOMO \rightarrow LUMO transition, so all of the calculations of k_r and k_{nr} are feasible to apply TDDFT. Moreover, based on the electronic structure parameters of both the compounds, the normal mode displacements, Huang–Rhys factor, and nonadiabatic electronic coupling between the two electronic states were calculated; the radiative and nonradiative decay rates were further determined; and the fluorescent quantum yield was also obtained.

3. RESULTS AND DISCUSSION

3.1. Geometry and Normal Mode Analysis. Both the TTM-3NCz and TTM-3PCz molecules (Figure 1) can be

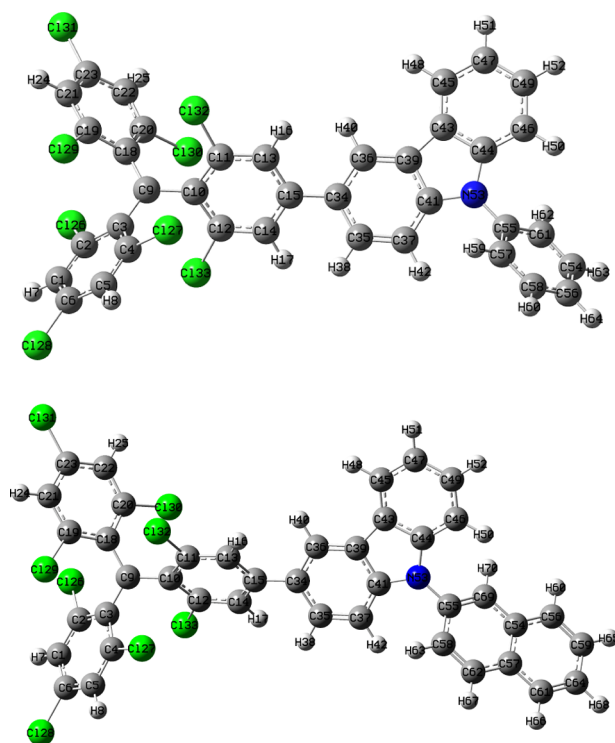


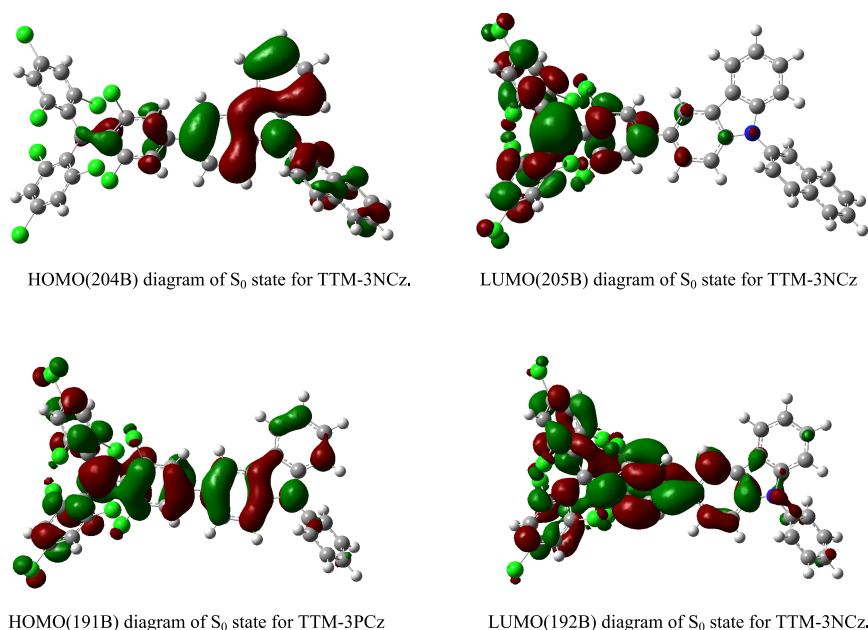
Figure 1. Structure of the TTM-3PCz (top) and TTM-3NCz molecules (bottom).

divided into three moieties, i.e., a tris(2,4,6-trichlorophenyl) methyl (TTM) fragment, a carbazole fragment, and a naphthyl or phenyl fragment. The parts calculating bond lengths, bond angles, and dihedral angles of S_0 and S_1 for the TTM-3NCz and TTM-3PCz molecules are given in Table 1. By comparing the bond parameters between the S_0 and S_1 states, one can see that the largest change of bond length appears in C20–Cl30 at the TTM group; it is 0.0124 Å for TTM-3NCz, while for

TTM-3PCz, it is 0.0122 Å. The above change could be understood from the diagram of the frontier molecular orbitals (all of the highest occupied molecular orbital (HOMO) and lowest occupied molecular orbital (LUMO) diagrams are shown in Figure 2). One can see that the electron density on HOMO is mainly distributed on the carbazole fragment, while that on LUMO is distributed mainly on the TTM fragment. As an electron is excited from the HOMO to LUMO, the distribution of the electron density on TTM for S_1 is greater than that for S_0 , and as a result, the bond lengths of the ground states are longer than those of the excited states. The change of the C18–C19 bond in the TTM group is second only to the C20–Cl30 bond and also beyond 0.01 Å; for the C15–C34 bond, which bonds TTM to the carbazole fragment, 0.0068 Å difference exists in TTM-3NCz and 0.0096 Å difference exists in the TTM-3PCz molecule. As to the C41–N53, C39–C43, and C44–N53 bonds belonging to the pyrrole ring in the carbazole, there are obvious changes compared with other covalent bonds listed in Table 1. It seems that the bonds of both the chlorobenzol rings, which are nonadjacent to carbazole, are lengthened in the S_1 state based on $\Delta(S_0 - S_1)$, i.e., the $\Delta(S_0 - S_1)$ values of C18–C19, C18–C20, and C19–Cl29 are negative. On the contrary, another chlorobenzol ring, which is adjacent to the carbazole, is shortened, i.e., the $\Delta(S_0 - S_1)$ values of C12–C14 and C14–C15 are positive; at the same time, the naphthyl or phenyl fragment becomes longer too. As for the carbazole, some bonds stretch and some shrink, due to the irregular delocalization of the π orbital in the carbazole, and the change of the bond lengths is also irregular. All of the bond angles shown in Table 1 have not changed significantly from the ground state to the excited state, and the differences of all of the listed bond angles do not exceed 0.8°. However, there are distinct changes in the dihedral angles between the S_0 and S_1 states. The main difference is found to be at the dihedral angle between both the chlorobenzene rings in the TTM unit and the variation beyond 6°, and the obvious variation of the other dihedral angle between the naphthyl and carbazole fragments is close to 10°. The above data show that the electrons will redistribute on all of the molecules in S_1 states and the excited geometry will be reorganized to keep minimum energy. It is well known that the displacement of mode between the initial state and final state can reflect the change of molecular geometry. For this reason, all of the vibrational modes were investigated and the contribution of each of them to the displacement between S_0 and S_1 states was presented. The selected frequencies of normal modes and displacement of modes for all of the S_0 and S_1 states are reported in Table 4 (for TTM-3NCz) and Table S2 (for TTM-3PCz). As one can see that regardless of TTM-3NCz or TTM-3PCz, the 10 vibration modes with the lowest frequencies contribute the largest displacement between S_0 and S_1 ; these modes belong to the rotations of the TTM fragment, carbazole, and phenyl (or naphthyl) ring. The range of frequencies for TTM-3NCz S_1 is from 8.32 to 51.22 cm^{-1} , which are slightly higher than those of TTM-3PCz S_1 (from 4.53 to 48.22 cm^{-1}). Figure 4 visually shows that the high- and moderate-frequency modes, which correspond to C–H and C–C single bond and C=C and C=N double bond stretching vibrations, contribute very small displacements; in stark contrast, the low-frequency modes of TTM-3NCz and TTM-3PCz present more large displacement. To lower excited energy dissipation, we can prevent the rotations of these fragments by the steric hindrance effect or other intermolecular

Table 1. Selected Bond Lengths (Å), Angles, and Dihedral Angles (in deg) in the Optimized S_0 and S_1 States for TTM-3NCz and TTM-3PCz

	TTM-3NCz				TTM-3PCz		
	S_0	S_1	$\Delta(S_0 - S_1)$		S_0	S_1	$\Delta(S_0 - S_1)$
C9–C10	1.4698	1.4680	0.0018	C9–C10	1.4699	1.4695	0.0004
C15–C34	1.4812	1.4744	0.0068	C15–C34	1.4812	1.4716	0.0096
C55–N53	1.4247	1.4184	0.0063	C55–N53	1.4253	1.4248	0.0005
C20–Cl30	1.7543	1.7667	−0.0124	C20–Cl30	1.7543	1.7665	0.0122
C19–Cl29	1.7546	1.7614	−0.0068	C19–Cl29	1.7546	1.7610	−0.0064
C18–C20	1.4197	1.4278	−0.0081	C18–C20	1.4197	1.4276	−0.0079
C18–C19	1.4193	1.4302	−0.0109	C18–C19	1.4193	1.4303	−0.011
C14–C15	1.4036	1.4018	0.0018	C14–C15	1.4036	1.4033	0.0003
C12–C14	1.3884	1.3879	0.0005	C12–C14	1.3884	1.3871	0.0013
C41–N53	1.3934	1.3914	0.002	C41–N53	1.3938	1.3842	0.0096
C44–N53	1.4009	1.4051	−0.0042	C44–N53	1.4002	1.4056	−0.0054
C39–C43	1.4494	1.4585	−0.0091	C39–C43	1.4493	1.4579	−0.0086
C43–C44	1.4189	1.4168	0.0021	C43–C44	1.4189	1.4162	0.0027
C39–C41	1.4198	1.4205	−0.0007	C39–C41	1.4198	1.4236	−0.0038
C55–C58	1.4216	1.4219	−0.0003	C55–C57	1.4004	1.4007	−0.0003
C55–C69	1.3801	1.3849	−0.0048	C55–C61	1.4005	1.4007	−0.0002
C10–C9–C18	120.14	119.43	0.71	C10–C9–C18	120.10	119.36	0.74
C3–C9–C10	120.12	119.42	0.70	C3–C9–C10	120.14	119.37	0.77
C15–C34–C35	120.65	120.79	−0.14	C15–C34–C35	120.43	120.75	−0.32
C41–N53–C55	125.62	125.70	−0.08	C41–N53–C55	125.77	125.69	0.08
C44–N53–C55	125.96	125.46	0.5	C44–N53–C55	125.80	125.35	0.45
C58–C55–C69	120.30	120.72	−0.42	C57–C55–C61	120.05	120.67	−0.62
C3–C9–C18–C20	−130.93	−136.99	6.06	C3–C9–C18–C20	−130.98	−137.24	6.26
C3–C9–C10–C11	−132.66	−130.92	−1.74	C3–C9–C10–C11	−132.65	−130.26	−2.39
C18–C9–C10–C11	47.33	49.02	−1.69	C18–C9–C10–C11	47.35	49.71	−2.36
C13–C15–C34–C35	144.60	146.96	−2.36	C13–C15–C34–C35	144.45	148.27	−3.82
C41–N53–C55–C58	−61.16	−50.23	−9.93	C41–N53–C55–C57	−62.43	−54.20	−8.23

**Figure 2.** Frontier molecular orbital diagrams of TTM-3NCz and TTM-3PCz.

interactions, such as by introducing all sorts of groups on the title molecules to decrease molecular deformation.

On the basis of the optimized S_0 and S_1 minima, the emission spectra of the title free radical molecules were theoretically investigated. The detailed electronic excitation energies, configuration coefficients, and oscillator strengths are

listed in Table 2. It is found that the configuration coefficient of 204B (HOMO) \rightarrow 205B (LUMO) for the S_1 state of TTM-3NCz is 97.16% and that of 191B (HOMO) \rightarrow 192B (LUMO) of TTM-3PCz is 96.95%. These single HOMO and LUMO diagrams display the π and π^* characteristics as shown in Figure 2, which indicates the intersystem crossing process

Table 2. Emission Data of TTM-3NCz and TTM-3PCz According to TDDFT, Together with the Experimental Data

compound	oscillator strength	main configuration	assignment	λ_{cal} (nm)	$\lambda_{\text{exp-PL}}$ (nm)	a Debye
TTM-3NCz	0.1280	204B \rightarrow 205B	0.9716	709.80	707	5.8648
		203B \rightarrow 205B	0.1057			
		201B \rightarrow 205B	−0.1462			
TTM-3PCz	0.1281	191B \rightarrow 192B	0.9695	701.65	695	5.8631
		189B \rightarrow 192B	−0.1720			
The Predicted Emission Data of the TTM-3NCz Dimer, TTM-3PCz Dimer, and the Perfluorinated TTM-3NCz Molecule						
dimer of TTM-3NCz	0.0838	402B \rightarrow 409B	−0.1077	721.05		
		408B \rightarrow 409B	0.9814			
dimer of TTM-3Pcz	0.0669	382B \rightarrow 383B	0.9867	711.88		
TN-F ₈	0.1639	173A \rightarrow 175A	−0.2403	610.10		5.2012
		169B \rightarrow 173B	−0.1605			
		171B \rightarrow 173B	0.1296			
		172B \rightarrow 173B	0.9211			

^aTransition electric dipole moments between the ground and excited states, the electric dipole moment is 5.9544 for the ground state of TTM-3NCz, 5.6760 for the ground state of TTM-3PCz, and 4.8845 D for the ground state of TN-F₈.

Table 3. Selected Frequency (freq/cm^{−1}), Displacement (D/au), Huang–Rhys Factors (HR), Franck–Condon Factors (FC), and Nonadiabatic Electronic Coupling (V_i/cm^{-1}) for the First Excited State of the TTM-3NCz Molecule

freq (S_1 state)	D	HR	FC	V_i	freq (S_1 state)	D	HR	FC	V_i
8.32	−95.00	0.17	0.10	74.30	249.74	7.43	0.03	0.03	225.57
10.65	43.87	0.05	0.04	108.36	255.93	−9.37	0.05	0.05	336.43
15.46	126.00	0.56	0.10	247.34	289.10	3.01	0.01	0.01	289.71
26.99	123.83	0.94	0.14	307.64	299.00	2.99	0.01	0.01	43.44
32.17	−6.74	0.00	0.00	322.83	413.21	3.81	0.01	0.01	539.92
34.52	113.65	1.02	0.13	315.07	520.63	7.16	0.06	0.05	355.65
38.23	−46.59	0.19	0.13	73.97	525.74	−3.22	0.01	0.01	171.84
44.51	184.80	3.46	0.00	201.60	701.35	4.15	0.03	0.03	82.79
51.22	140.22	2.29	0.02	191.35	715.57	−2.20	0.01	0.01	342.21
52.33	−57.01	0.39	0.18	179.98	782.38	−11.95	0.25	0.15	2.14
67.79	15.49	0.04	0.03	130.13	945.09	−1.71	0.01	0.01	197.29
74.09	−4.26	0.00	0.00	272.60	1050.40	5.38	0.07	0.06	30.04
81.60	9.45	0.02	0.02	214.64	1065.94	−3.65	0.03	0.03	308.94
114.19	−8.39	0.02	0.02	153.76	1180.97	3.44	0.03	0.01	71.84
134.74	7.16	0.02	0.02	259.28	1182.53	−1.33	0.00	0.00	153.42
143.38	−5.50	0.01	0.01	102.81	1187.93	−2.35	0.02	0.01	53.85
145.41	7.59	0.02	0.02	449.76	1207.86	−4.41	0.05	0.05	20.70
150.48	−6.17	0.01	0.01	79.59	1274.91	2.69	0.02	0.02	5.01
155.03	21.88	0.17	0.12	44.48	1314.40	−0.96	0.00	0.00	623.67
156.88	−6.48	0.01	0.01	87.30	1454.52	−4.05	0.05	0.05	466.67
162.55	−6.66	0.02	0.02	123.00	1608.78	−0.96	0.00	0.00	700.92
172.83	13.44	0.07	0.06	464.44	1613.99	−2.20	0.02	0.01	131.05
207.97	11.55	0.06	0.06	261.94	1662.17	−1.90	0.01	0.01	126.65
219.81	18.30	0.17	0.12	747.90	3206.63	−0.99	0.01	0.01	11.68

can be ignored due to lack of $n \rightarrow \pi$ transition, thus the internal conversion becomes mainly nonradiative channels of dissipating energy for excited state.¹⁶ The largest calculated emission peak (λ_{cal}) for TTM-3NCz is 709.8 nm with the oscillator strength 0.1280 and the experimental one ($\lambda_{\text{exp-PL}}$) is 707 nm; as to TTM-3PCz, the λ_{cal} is 701.65 nm with the oscillator strength 0.1281 and the $\lambda_{\text{exp-PL}}$ is 695 nm. The above data show that both the calculated values are consistent with the observed values, which implies that the method is suitable for the molecular systems.

In comparison, several other functionals (PBE0, CAM-B3LYP, M06, ω B97XD, and HF) with different Hartree–Fock components are employed to obtain the absorption and emission data (listed in Table S1) with the 6-31+G(d) basis set. It is found that the absorption and emission wavelengths

change significantly when functionals are different, and the data calculated by B3LYP happened to be in good agreement with experimental values. Thus, B3LYP is adopted in all of the following calculations in this work.

3.2. Photophysical Properties. The nonadiabatic coupling term V_b , which results from vibrational and electronic interactions in a molecule for all of the normal modes, has been implemented by the MOMAP package, and selected data with relatively large couplings are given in Table 3. The normal vibrational frequencies, the Huang–Rhys factor (HR), and the Franck–Condon (FC) factors are listed together. In the S_1 state of TTM-3NCz, the displacement of the modes with 15.46, 26.99, 34.52, 44.51, 51.22 cm^{−1} exceeds 100 au, due to the relation of the Huang–Rhys (HR) factor and the displacement (D), $\text{HR}_j = (v_j D_j^2)/2h$; thus, these modes have

more large HR values. Therefore, they are the main channels for determining the internal conversion rate.²³ The largest HR factor for the TTM-3NCz molecule is 3.46 corresponding to the vibrational mode with 34.52 cm^{-1} . It is assigned to the twisted vibration of aromatic rings, as shown in Figures 3 and

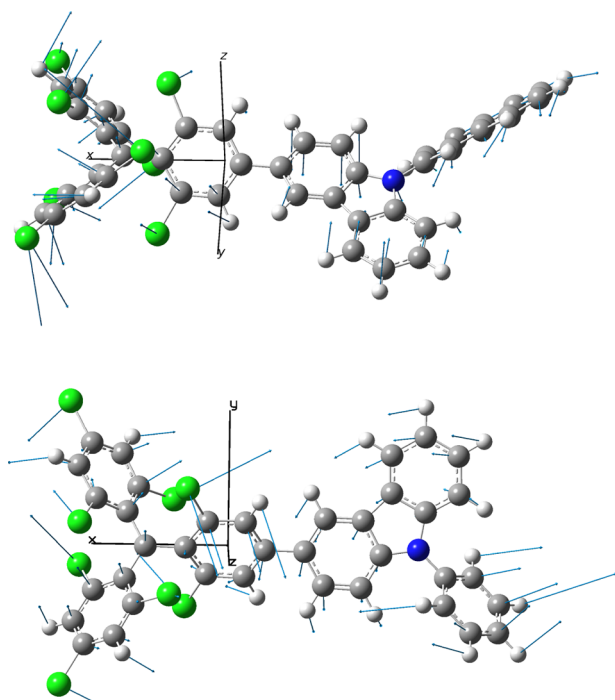


Figure 3. Scheme of the largest normal mode displacement vectors for the first excited state of the TTM-3NCz (top) and TTM-3PCz (bottom) molecules.

4. As regards the TTM-3PCz molecule, the vibrational modes with low frequencies are similar to TTM-3NCz; for example, the displacements of the modes with $8.54, 24.31, 34.92, 48.22, 51.32\text{ cm}^{-1}$ exceed 100 au too. The largest HR factor for the TTM-3PCz molecule is 2.18 corresponding to the 48.22 cm^{-1} vibrational mode; it is also assigned to the twisted vibration of aromatic rings in Figure 3.

Furthermore, the radiative decay rate (k_r) and nonradiative decay rate (k_{nr}) for both the TTM-3NCz and TTM-3PCz molecules were obtained theoretically and are listed in Table 4. One can observe from Table 3 that (i) the calculated k_r values of TTM-3NCz and TTM-3PCz are $4.53 \times 10^7\text{ s}^{-1}$ and 3.85×10^7 at room temperature and the corresponding lifetimes are 22.1 and 26.0 ns, respectively, which are consistent well with the observed value 17.2 ns for the TTM-3NCz molecule and 21.2 ns for the TTM-3PCz molecule, this indicates that the method to predict the radiative decay is reasonable; (ii) the calculated k_{nr} values are 2 orders of magnitude higher than the k_r values at room temperature, which implies that the fluorescence quantum efficiency is very low and much less than the experimental result; Shuai et al. pointed out that the nonadiabatic coupling is easily influenced by the external environmental factors, such as the polarity of the solvent, the steric hindrance, and the different molecule packings;¹⁶ meanwhile, the Duschinsky effect influences k_{nr} dramatically,¹⁸ and the experimental data are from the thin film comprising TTM-3NCz and TTM-3PCz molecules and other charge transport materials,¹³ so the calculated k_{nr} values are inaccurate; (iii) the change of k_r is insensitive to the decrease

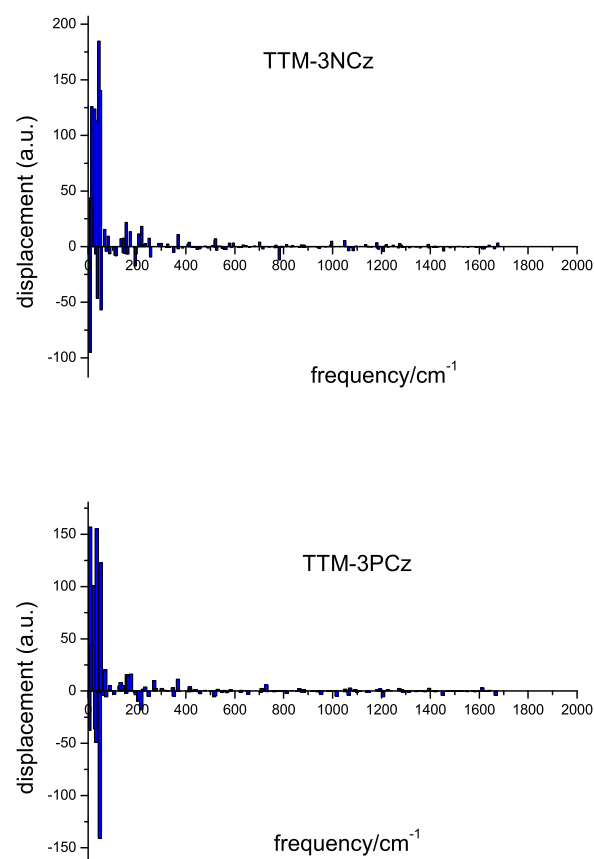


Figure 4. Calculated displacement versus the normal mode for (top) the TTM-3NCz molecule and (bottom) the TTM-3PCz molecule.

of the temperature; in contrast, the k_{nr} values are sensitive to the temperature and their change is apparent, which shows that the fluorescence quantum efficiency of the TTM-3NCz molecule will increase distinctly compared with the TTM-3PCz molecule; (iv) obviously, there are more atoms in a TTM-3NCz molecule compared with TTM-3PCz, and the corresponding vibrational modes of a TTM-3NCz molecule are more than those of the TTM-3PCz molecule. However, the calculated nonadiabatic coupling about the TTM-3NCz molecule is $19\,964\text{ cm}^{-1}$ and the counterpart about the TTM-3PCz molecule is $20\,135\text{ cm}^{-1}$ (all of the V_i values and frequencies are listed in Table S3). Therefore, the k_{nr} of the TTM-3PCz molecule at different temperatures is larger than that of the TTM-3NCz molecule accordingly, although the latter possesses more channels of internal conversion, which implies that the predicted fluorescence quantum efficiency of the TTM-3NCz molecule is always larger than the one of the TTM-3PCz molecule.

Table 4 shows that the k_r of TTM-3NCz at 300 K is $4.53 \times 10^7\text{ s}^{-1}$ when the Duschinsky effect is considered, while the k_{nr} is $3.96 \times 10^{10}\text{ s}^{-1}$. The former plummets about 3 orders of magnitude compared with the latter, and the k_{nr} is far greater than the k_r ; nevertheless, when the Duschinsky effect is ignored, the k_r of TTM-3NCz at the same temperature reduces to $5.24 \times 10^6\text{ s}^{-1}$ and the k_{nr} becomes $7.18 \times 10^6\text{ s}^{-1}$. We can see that both of them decrease in contrast to the data with the Duschinsky effect and have the same order of magnitude. In addition, it is found that the k_r of TTM-3NCz with the Duschinsky effect possesses less variation range compared to the k_r without the Duschinsky effect. In stark contrast, the

Table 4. Calculated Radiative Decay Rate (k_r) and Nonradiative Decay Rate (k_{nr}) from S_1 to S_0 and the Corresponding Fluorescence Quantum Yield (η) at Different Temperatures for TTM-3NCz and TTM-3PCz Molecules

TTM-3NCz				TTM-3PCz			
T/K	k_r/s^{-1}	k_{nr}/s^{-1}	η	T/K	k_r/s^{-1}	k_{nr}/s^{-1}	η
300	4.53×10^7	3.96×10^{10}	0.11%	300	3.85×10^7	9.18×10^{10}	0.042%
200	7.94×10^7	1.69×10^{10}		200	8.39×10^7	5.43×10^{10}	
100	8.14×10^7	2.22×10^9		100	8.61×10^7	1.24×10^{10}	
50	8.24×10^7	1.64×10^8		50	8.71×10^7	1.12×10^9	
no Duschinsky effect							
300	5.24×10^6	7.18×10^6	41.8%	300	3.27×10^6	3.97×10^6	45.2%

variation of the k_{nr} is significant with and without the Duschinsky effect (from 3.96×10^{10} to 7.18×10^6 s $^{-1}$). The changing trends for the TTM-3PCz molecule are the same, but with different degrees of variations (k_r is 3.85×10^7 s $^{-1}$ and k_{nr} is 9.18×10^{10} s $^{-1}$ with the Duschinsky effect, k_r is 3.27×10^6 s $^{-1}$ and k_{nr} is 3.97×10^6 s $^{-1}$ without the Duschinsky effect at 300 K). This is because formula 5 contains the nonadiabatic transition momentum R_{kl} , which includes both diagonal and nondiagonal terms to calculate the k_{nr} . When taking the Duschinsky effect into account, the nondiagonal term increases significantly; thus, the nonradiative rate also increases. If not, there is only the diagonal term in R_{kl} without the Duschinsky mixing effect, so the k_{nr} decreases, but for formula 4 to calculate the radiative rate, it refers to the integral of the emission spectrum, and the change of the integral area is minor with the Duschinsky mixing effect.¹⁸ As a result, the Duschinsky effect on the k_r is not significant.

If we do not consider the Duschinsky mixing effect, the fluorescence quantum yield for TTM-3NCz increases dramatically from 0.11 to 41.8% and for TTM-3PCz from 0.042 to 45.2%, which happen to reach the same order of magnitude compared with the experimental data. Besides the influence of the nonadiabatic transition momentum R_{kl} , there are three other possible reasons in the case as follows: first, the calculated excited energy is underestimated for open-shell systems due to spin contamination;^{24,25} second, for the optimized geometry of the excited state and the adiabatic energy, there exists some error because TDDFT is a single-configuration approximation method instead of a multi-configuration method,^{26,27} and the errors derived from the above may offset each other. Finally, both the title molecules are surrounded by other materials in OLED. The steric hindrance from these materials results in a higher rigidity of both the radical emitters; moreover, an ingredient of the displaced harmonic oscillator increases and the distorted displaced harmonic oscillator decreases. It seems that the Duschinsky effect between the ground state and the first excited state can be ignored.¹⁸

3.3. Simulated Fluorescence Spectrum of TTM-3NCz Using the Distorted and Displaced Harmonic Oscillator Model at Room Temperature. At the S_1 minima, the HOMO–LUMO is predominantly responsible for the $S_1 \rightarrow S_0$ electronic de-excitation transition (weight of TTM-3NCz, 97.16% and TTM-3NPz, 96.95%), and the calculated maximum peak of $S_1 \rightarrow S_0$ at the emission spectrum for the TTM-3NCz molecule appears in the $0 \rightarrow 0$ transition, which is 1.75 eV (709 nm). To get a band spectrum instead of a line spectrum, we simulated the emission spectrum of TTM-3NCz using the correlation function method (eq 3), and the total time interval for the correlation function is set to [−1000 fs, 1000 fs], with a time increment, Δt , of 0.01 fs. For the

calculation of the vibronic spectrum, all of the vibrational modes have been included and the Duschinsky effect, which is derived from the difference between the frequencies of the ground state and the excited state, has also been considered.^{28,29} The simulated fluorescence spectrum of TTM-3NCz containing a contribution of the FC factor is shown in Figure 5, where two emission peaks can be seen in the spectrum: one is main peak corresponding to the $0 \rightarrow 0$ transition and the other is a shoulder peak coming from the contribution of the FC factor. Obviously, the intensity of the

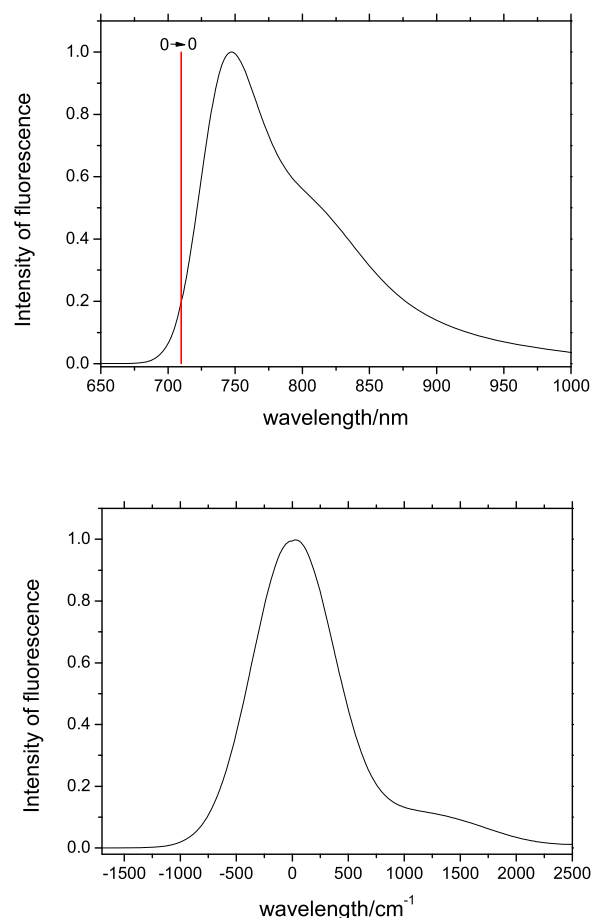


Figure 5. Simulated fluorescence spectrum of TTM-3NCz using the distorted harmonic oscillator model at room temperature (top). The emission peak at 709.8 nm is corresponding to the $0 \rightarrow 0$ transition, and the maximum λ_{cal} changes from 709.8 to 747.7 nm with the Duschinsky effect. The simulated fluorescence spectrum of TTM-3NCz using the displaced harmonic oscillator model at room temperature (bottom). The maximum λ_{cal} has a red shift of 50 cm $^{-1}$ without the Duschinsky effect.

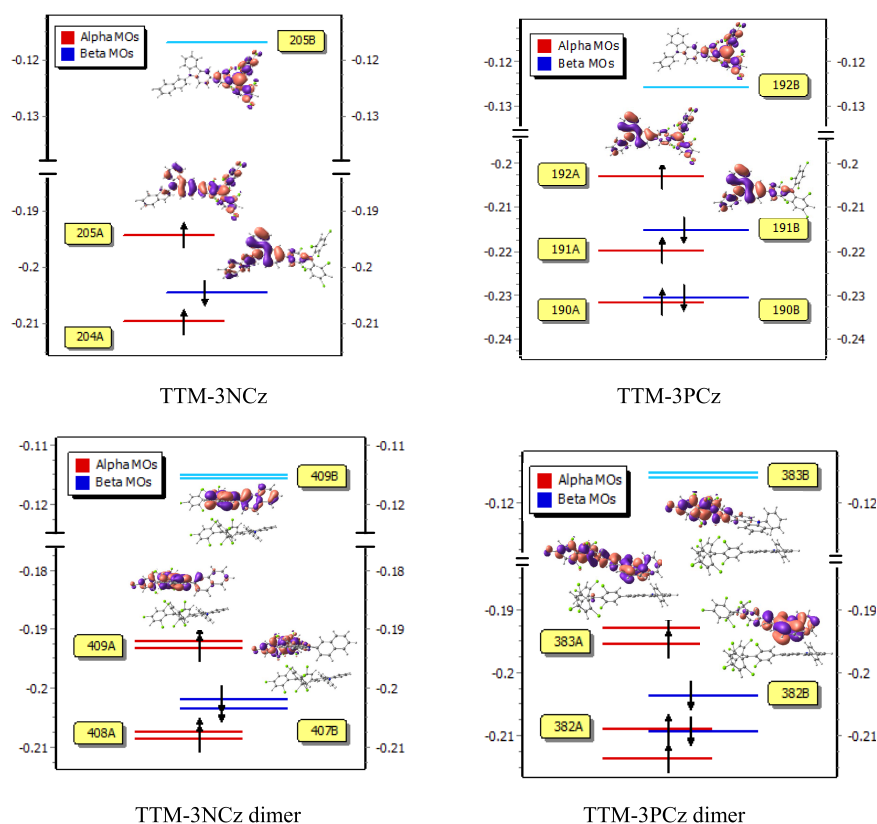


Figure 6. Molecular orbital levels with au for TTM-3NCz, TTM-3PCz, and their dimers at the B3LYP/6-31+G(d) level.

main peak is far stronger than that of the shoulder peak. Whether the peak position or peak shape of the simulated emission spectrum employed the correlation function, our calculated results are consistent with the observed spectrum, which indicated that the distorted harmonic oscillator model can well describe the spectral characteristics.

To further understand the appearance of the shoulder peak in the fluorescence spectrum, we also calculated the approximate FC factor of each normal mode.³⁰ On the basis of the harmonic oscillator model, the FC factor of each mode can be expressed by a Poisson distribution as follows

$$\prod_k |\langle \theta_{f_k} | \theta_{i0} \rangle|^2 = \prod_k \frac{S_k^{v_k}}{v_k!} e^{-S_k} \quad (6)$$

For both the electronic states of a molecule, there is a small displacement in the potential energy surface using the harmonic oscillator model. For simplicity, the contribution to the spectrum of the $0 \rightarrow 0$ and $0 \rightarrow 1$ vibrational transitions has been considered and other transitions are ignored; thus, the FC factor of vibrational modes is simplified as $S_k e^{-2S_k}$ for each mode and all of the data are listed in Table 3 and S2. As can be seen that the FC factors with low frequencies, 8.32, 15.46, 26.99, 34.52, 38.23, 52.53 cm^{-1} , are considerably large, these normal modes significantly impact on the shape of the emission spectrum. In addition, because the peak will spread with FWHM in the Gaussian spectrum, the effect of the low-frequency modes will overlap with the main peak (corresponding to the $0 \rightarrow 0$ electron transition), which makes the emission peak frequency red-shift about 50 cm^{-1} . The 782.38, 995.82, 1050.40, and 1207.86 cm^{-1} modes, which are assigned to the breathing vibration of the naphthalene ring, deformation vibration of the naphthalene ring, twisted vibration of the

naphthalene ring, and H atom rocking vibration of the benzene rings in place, have a significant impact on the spectrum, which leads to the appearance of a shoulder peak in the emission spectrum, it entirely corresponds with the shape of the emission spectrum in nonpolar solvent cyclohexane. Figure S1 shows the simulated fluorescence spectrum of TTM-3PCz using the distorted and displaced harmonic oscillator model at room temperature, which has the same spectral shape as that of the TTM-3NCz molecule.

3.4. Electronic Structure and Fluorescent Property of Dimers.

As is well known that free radical molecules are generally unstable,³¹ two free radicals tend to form a dimer by the central head-to-head C–C bond to attenuate reactivity.^{32,33} Thus, we investigated the dimers composed of both the title molecules. To obtain the stable geometry of the dimer of TTM-3NCz and TTM-3PCz, the relaxing potential energy scan was performed at the UB3LYP/6-31+G(d) level for each dimer. The scanning along the molecular horizontal axis and the vertical direction was executed to confirm the spatial position of both the molecules in a dimer. Then, making both the molecules rotate each other to get the geometry with minimum of energy, finally, the dimer was optimized based on this geometry again using UB3LYP/6-31+G(d). Figure S2 illustrates the optimized geometries of both the conformations of the TTM-3NCz and TTM-3PCz dimers; moreover, based on the application of the counterpoise correction for the basis set superposition error,^{34,35} the binding energies of the single molecules in the dimer are -5.01 kJ/mol for TTM-3NCz and -5.23 kJ/mol for TTM-3PCz. The calculated data imply that both the free radicals do not form C–C bonds due to the stereo-hindrance effect of chlorobenzene; nevertheless, the total energy decreases during the formation of dimer systems

and there is a chance that this effect exists in the optoelectronic device. Therefore, the electronic structures and fluorescent properties of both the dimers were further explored.

The energy levels of both the TTM-3NCz and TTM-3PCz single molecules and their dimers, low-lying states, based on the optimized geometry are shown in Figure 6. For the TTM-3NCz dimer, the HOMO is 409A and 410A, respectively, which mainly delocalized over the TTM and the dibenzopyrrole moiety, while the LUMO is distributed on the naphthalene ring and dibenzopyrrole moiety. Similarly, the HOMO (205A) of the single TTM-3NCz molecule is mainly distributed on dibenzopyrrole and TTM moieties. Meanwhile, the LUMO of the single molecule is localized on the TTM moiety. As for the dimer composed of both TTM-3PCz molecules, the HOMO is 383A and 384A, respectively, the electronic density of each orbital belongs to the different molecule and is distributed on all of the molecules. Meanwhile, the LUMO (385B) localizes on the TTM unit. In comparison, there is hardly any change between the frontier orbitals of the dimer and ones of the single TTM-3PCz molecule, which once again demonstrates that both the dimers have no significant interaction between two single molecules.

It is found that the 408B \rightarrow 409B transitions mainly contribute to the first excited state for the TTM-3NCz dimer. This transition configuration accounts for 98% of the total listed in Table 2. Both the orbitals involving the fluorescence emission process belong to the same molecule in the dimer. Obviously, both HOMO (408B) and LUMO (409B) cannot effectively overlap each other, as observed from Figure 6; thus, the oscillator strength is only 0.0838. The maximum emission wavelength is 729 nm at the UB3LYP/6-31+G(d) level for the dimer, which shows an about 20 nm red shift compared with the maximum one (708 nm) of the single molecule. Regarding the transition of the TTM-3PCz dimer in the fluorescence emission process, the 382B \rightarrow 383B transition is dominant and accounts for almost 100%, and the maximum emission peak with oscillator strength 0.0669 is 711 nm. Compared to the transition of the single TTM-3PCz molecule, the dimer shows a red shift of 10 nm.

The natural transition orbitals (NTOs) of S_1 states for both the TTM-3NCz and TTM-3PCz molecules are illustrated in Figure 7, which provides a dramatic simplification in the qualitative description of an electronic transition.^{36,37} The

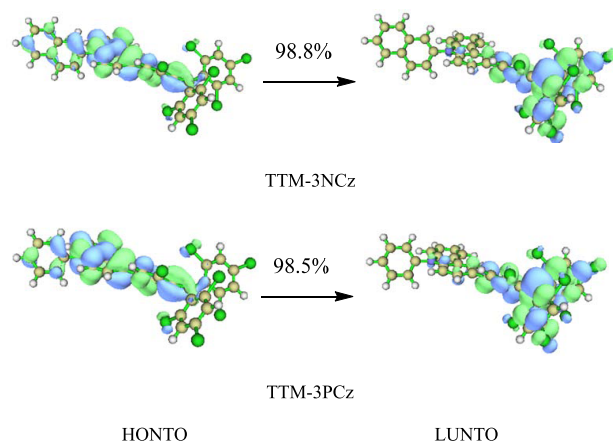


Figure 7. Transition characteristics of the natural transition orbitals for the single molecules.

highest occupied natural transition orbital (HONTO) of both the single molecules is localized in dibenzopyrrole, and the lowest unoccupied natural transition orbital (LUNTO) mainly concentrates at the TTM moiety. The HONTO \rightarrow LUNTO transition of TTM-3NCz accounts for 98.8% of the total and that of TTM-3PCz is 98.5%. The contribution of each atom to these orbitals can be obtained by the Multiwfn code as well.³⁷ For HONTOs of both the molecules, the main contribution comes from these atoms in the dibenzopyrrole unit. Nevertheless, for their LUNTOs, besides the contribution of the benzene ring in the TTM unit, the center C atom in TTM also plays an important role; it accounts for 34.4% of the total for the TTM-3NCz dimer and 34.0% for the TTM-3PCz dimer, which exhibits the typical p electron characterization, so this excitation characteristic can be referred to as $\pi \rightarrow p^*$.

Whether the TTM-3PCz dimer or TTM-3NCz dimer, their oscillator strengths are far smaller than those of their respective single molecules, while the emission energies of both the dimers are close to those of the single molecules. Based on Einstein's spontaneous emission equation, the radiative rate is related not only to the orbital overlap (the larger the orbital overlap, the larger the oscillator strength) but also to the square of the energy difference between the excited state (S_1) and the ground state (S_0), and it can be simplified as follows³⁸

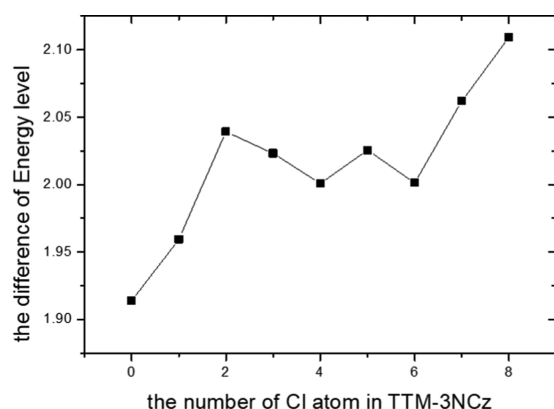
$$k_r = \frac{f \Delta E_{ij}^2}{1.499 \text{ cm}^{-2} \cdot \text{s}} = A f \Delta E_{ij}^2 \quad (7)$$

here, f is the oscillator strength of the first excited state (S_1) and ΔE_{ij} is the emission energy, the calculated $k_r(\text{TTM-3NCz})/k_r(\text{TTM-3NCz dimer})$ is 1.61, and $k_r(\text{TTM-3PCz})/k_r(\text{TTM-3PCz dimer})$ is 1.97. Obviously, both the radiative rates are not so much different; nevertheless, the dimers possess more channels of internal conversion. The extra energy in excited dimers will be taken away easily by more vibration modes. It can be expected that the dimers make a little contribution to the fluorescence spectra.

3.5. Prediction for the Fluorinated TTM-3NCz Molecule. Due to the HOMO \rightarrow LUMO transition accounting for the vast majority proportion in the process of fluorescence emission for both the TTM-3NCz and TTM-3PCz molecules, one-electron approximation can be applied, i.e., the HOMO \rightarrow LUMO transition replaces the $S_1 \rightarrow S_0$ transition.^{39,40} Given that the gap of the frontier molecular orbital energy level has a major impact on the radiative rate based on one-electron approximation and formula 7, the electronic structure of the fluorinated TTM-3NCz molecules was investigated, in which the fluorine atom substitutes the chlorine atom on the TTM unit in turn. Thus, there are eight substituted compounds, and these compounds contain different numbers of fluorine and chlorine atoms. For simplicity, we write them $\text{TN-F}_i\text{Cl}_7$, which means one chlorine atom is substituted by one fluorine atom, the remaining seven chlorine atoms in the TTM moiety, $\text{TN-F}_2\text{Cl}_6$, $\text{TN-F}_3\text{Cl}_5$, etc., the meaning is the same as above. All of the compounds were optimized using UB3LYP/6-31+G(d), and their energy levels and gaps of the frontier orbitals are listed in Table 5. One can see in Figure 8 that the gaps increase with chlorine atoms anchoring to benzene rings; however, the gaps of the frontier orbitals become irregular when the number of substituent Cl atoms are 3, 4, 5, and 6. The minimum gap is 1.914 eV for perfluorinated TN-F_8 , the maximum gap is 2.109 eV for perchlorinated TTM-3NCz, and the difference between both the compounds is about 0.195 eV, which corresponds to

Table 5. Frontier Orbital Energy Level (au) and the Energy Level Gap (eV) of Fluorinated TTM-3NCz

compound	orbital	energy (au)	energy level gap (eV)
TN-F ₈	HOMO	−0.17422	1.914
	LUMO	−0.10389	
TN-F ₇ Cl ₁	HOMO	−0.17629	1.959
	LUMO	−0.10428	
TN-F ₆ Cl ₂	HOMO	−0.17827	2.039
	LUMO	−0.10333	
TN-F ₅ Cl ₃	HOMO	−0.17989	2.023
	LUMO	−0.10554	
TN-F ₄ Cl ₄	HOMO	−0.18236	2.001
	LUMO	−0.10883	
TN-F ₃ Cl ₅	HOMO	−0.18465	2.025
	LUMO	−0.11021	
TN-F ₂ Cl ₆	HOMO	−0.18636	2.001
	LUMO	−0.11281	
TN-F ₁ Cl ₇	HOMO	−0.19063	2.062
	LUMO	−0.11486	
TTM-3NCz	HOMO	−0.19442	2.109
	LUMO	−0.11691	

**Figure 8.** Difference of the frontier orbitals for all fluorinated TTM-3NCz molecules at the B3LYP/6-31+G(d) level.

60 nm wavelength change. Based on the above data, we expect that the emission wavelength can be tuned within the range of about 60 nm, maybe infrared optical materials with doublet and efficiency will be able to be found. Moreover, the radiative rate k_r of the perchlorinated TTM-3NCz molecule is predicted to be the largest in all of the compounds due to the maximum gap. However, the calculated result indicates that the outcome is almost diametrically opposite to what has been predicted above. The wavelength of the maximum emission for the perfluorinated TN-F₈ is 610.10 nm with the oscillator strength 0.1639, and the difference is about 99.7 nm compared with the single TTM-3NCz molecule. The oscillator strength and the emission energy of TN-F₈ are larger than those of TTM-3NCz. The above facts suggest that TN-F₈ is an orange luminescent material rather than an infrared optical material. Perhaps, we can elucidate the above fact by the corresponding dipole moment and the transition configuration. The dipole moment of the first excited state for TN-F₈ is 5.20 D, which is about 90% of the dipole moment of the excited TTM-3NCz molecule (5.86 D), which implies that the extent of charge separation is smaller in the excited TN-F₈ molecule, thus the overlap of the HOMO and LUMO will be more efficient for the TN-F₈ molecule. This indicates that the oscillator strength

of TN-F₈ is larger. In addition, compared with the excited TTM-3NCz molecule, the main excited configurations for the TN-F₈ molecule in the emission process contain some transitions with more higher energy, such as 173A → 175A (the gap of the energy levels is 0.138 au), 169B → 173B (the gap is 0.134 au), 171B → 173B (the gap is 0.114 au), and 172B → 173B (the gap is 0.097 au); the main excited configurations for the TTM-3NCz molecule are 201B → 205B (the gap of the energy levels is 0.130 au), 203B → 205B (the gap is 0.105 au), and 204B → 205B (the gap is 0.089 au). The above data indicate that the energy difference between the S_1 and the S_0 states of the TN-F₈ molecule is larger than that of the TTM-3NCz molecule. As a result, the TN-F₈ emission energy is even greater, i.e., the maximum emission wavelength of the TN-F₈ molecule is smaller than that of the TTM-3NCz molecule. Moreover, due to the high oscillator strength and the emission energy, the radiative rate of the TN-F₈ molecule increases obviously compared with the TTM-3NCz molecule based on formula 5, which means that the fluorescence efficiency of the TN-F₈ molecule is probably even greater. The above calculated data show that the λ_{\max} (emission) of the TN-F₁Cl₇, TN-F₂Cl₆, TN-F₃Cl₅, TN-F₇Cl compounds changes from 610 to 710 nm, which provides an opportunity to select appropriate fluorescent materials with different colors. Finally, we predicted the stability of all the TN-F_mCl_n free radicals by the bond energy of their hydrides, and the specific discussion can be seen in the Supporting Information (in section The stability of the TN-F_mCl_n molecules). The calculated results suggest that the TTM-3NCz free radical is the most stable in all halogenated compounds because the chlorine atom can not only form a p- π conjugate system but also supply 3d orbitals to enlarge the delocalization space.⁴¹

4. CONCLUSIONS

In summary, we have theoretically studied the vibronic spectrum of the TTM-3NCz molecule employing a thermal vibration correlation function using the TDDFT method. The calculated results indicated that the main peak was impacted by the normal modes with lower frequencies and the shoulder peak of the emission spectrum was impacted by the middle-frequency modes. On the level of TDDFT, we investigated changes in the potential energy surfaces of the ground and excited states for TTM-3NCz and TTM-3PCz molecules. Both the calculated radiative decay rates were in good agreement with the observed data at room temperature, i.e., the calculated fluorescence lifetimes of both the species match with the experiment. It is noted that for the calculated nonradiative decay rates far away from the actual situation with the Duschinsky effect, there is a large deviation in the fluorescence quantum efficiency between the simulated and experimental data, which might be related to external factors and the nature of TDDFT; however, the fluorescence quantum efficiencies for both the compounds are in good agreement with the experimental data without the Duschinsky effect. Furthermore, the effect on the fluorescence, which comes from the dimers composed of the single title molecules, can be nearly eliminated due to the small binding energies. The predicted fluorescence property of the fluorinated TTM-3NCz molecule is perhaps better than that of the title compounds. With a change in the number of fluorine atoms in TTM, various multicolor luminescent materials can be exploited based on the parent TTM-3NCz.

■ ASSOCIATED CONTENT

■ Supporting Information

The Supporting Information is available free of charge at <https://pubs.acs.org/doi/10.1021/acs.jpca.9b10343>.

Theoretical method for the calculation of nonradiative decay rate; the stability of the halogenated TTM-3NCz molecules; figures of the simulated fluorescence spectrum of TTM-3PCz, optimized structures of the TTM-3NCz dimer, the bond energy of all of the hydrides for fluorinated TTM-3NCz molecules; tables of absorption and emission data of TTM-3NCz and TTM-3PCz by TDDFT; the part displacement, Huang–Rhys factors, and Franck–Condon factors for the first excited state of the TTM-3PCz molecule; the frequency (cm^{-1}) and nonadiabatic electronic coupling for the TTM-3NCz and TTM-3PCz molecules; and the total energy of fluorinated TTM-3NCz and the total energy and bond energy of hydrides (PDF)

■ AUTHOR INFORMATION

Corresponding Authors

Huixue Li – School of Chemical Engineering and Technology, Tianshui Normal University, Tianshui 741001, China; Phone: +86-15097274526; Email: li_hx2001@126.com

Zhifeng Li – School of Chemical Engineering and Technology, Tianshui Normal University, Tianshui 741001, China; Phone: +86-15097274526; Email: lizhfe2003@163.com

Other Authors

Xiaofeng Wang – School of Chemical Engineering and Technology, Tianshui Normal University, Tianshui 741001, China

Yuancheng Zhu – School of Chemical Engineering and Technology, Tianshui Normal University, Tianshui 741001, China

Complete contact information is available at: <https://pubs.acs.org/doi/10.1021/acs.jpca.9b10343>

Notes

The authors declare no competing financial interest.

■ ACKNOWLEDGMENTS

This work was supported by the Natural Science Foundation of China (No. 21463023), the Foundation Project of Beijing National Laboratory for Molecular Sciences (BNLMS20160155), the Research Fund of Education Department of Gansu Province (2016B-072), and the Key Projects of Tianshui Normal University (TSA1501). Thanks to the Key Laboratory of New Molecular Materials Design and Function of Gansu Province and the Key Subject of Theoretical Calculation in Tianshui Normal University.

■ REFERENCES

- (1) Lin, T. A.; Chatterjee, T.; Tsai, W. L.; Lee, W. K.; Wu, M. J.; Jiao, M.; Pan, K. C.; Yi, C. L.; Chung, C. L.; Wong, K. T.; Wu, C. C. Sky-Blue Organic Light Emitting Diode with 37% External Quantum Efficiency Using Thermally Activated Delayed Fluorescence from Spiroacridine-Triazine Hybrid. *Adv. Mater.* **2016**, *28*, 6976–6983.
- (2) Gómez-Bombarelli, R.; Aguilera-Iparraguirre, J.; Hirzel, T. D.; Duvenaud, D.; Maclaurin, D.; Blood-Forsythe, M. A.; Chae, H. S.; Einzinger, M.; Ha, D.-G.; Wu, T. Design of Efficient Molecular Organic Light-Emitting Diodes by a High-Throughput Virtual Screening and Experimental Approach. *Nat. Mater.* **2016**, *15*, 1120.
- (3) Cho, H.; Jeong, S. H.; Park, M.-H.; Kim, Y. H.; Wolf, C.; Lee, C. L.; Heo, J. H.; Sadhanala, A.; Myoung, N.; Yoo, S.; et al. Overcoming the Electroluminescence Efficiency Limitations of Perovskite Light-Emitting Diodes. *Science* **2015**, *350*, 1222–1225.
- (4) Ma, Y.; Zhang, H.; Shen, J.; Che, C. Electroluminescence from Triplet Metal–Ligand Charge-Transfer Excited State of Transition Metal Complexes. *Synth. Met.* **1998**, *94*, 245–248.
- (5) Uoyama, H.; Goushi, K.; Shizu, K.; Nomura, H.; Adachi, C. Highly Efficient Organic Light-Emitting Diodes from Delayed Fluorescence. *Nature* **2012**, *492*, 234–238.
- (6) Pope, M.; Swenberg, C. E. *Electronic Processes in Organic Crystals and Polymers*; Oxford University Press: New York, 1999.
- (7) Baldo, M. A.; O'Brien, D. F.; You, Y.; Shoustikov, A.; Sibley, S.; Thompson, M. E.; Forrest, S. R. Highly Efficient Phosphorescent Emission from Organic Electroluminescent Devices. *Nature* **1998**, *395*, 151–154.
- (8) Adachi, C.; Kwong, R. C.; Djurovich, P.; Adamovich, V.; Baldo, M. A.; Thompson, M. E.; Forrest, S. R. Endothermic Energy Transfer: A Mechanism for Generating Very Efficient High-Energy Phosphorescent Emission in Organic Materials. *Appl. Phys. Lett.* **2001**, *79*, 2082–2084.
- (9) Zhang, Q.; Bo, L.; Huang, S.; Nomura, H.; Tanaka, H.; Adachi, C. Efficient Blue Organic Light-Emitting Diodes Employing Thermally Activated Delayed Fluorescence. *Nat. Photonics* **2014**, *8*, 326–332.
- (10) Yuan, Y.; Chen, J. X.; Lu, F.; Tong, Q. X.; Yang, Q. D.; Mo, H. W.; Ng, T. W.; Wong, F. L.; Guo, Z. Q.; Ye, J.; et al. Bipolar Phenanthroimidazole Derivatives Containing Bulky Polyaromatic Hydrocarbons for Nondoped Blue Electroluminescence Devices with High Efficiency and Low Efficiency Roll-Off. *Chem. Mater.* **2013**, *25*, 4957–4965.
- (11) Jankus, V.; Snedden, E. W.; Bright, D. W.; Whittle, V. L.; Williams, J. A. G.; Monkman, A. Energy Upconversion Via Triplet Fusion in Super Yellow Ppv Films Doped with Palladium Tetraphenyltetraabenzoporphyrin: A Comprehensive Investigation of Exciton Dynamics. *Adv. Funct. Mater.* **2013**, *23*, 384–393.
- (12) Jankus, V.; Chiang, C. J.; Dias, F.; Monkman, A. P. Deep Blue Exciplex Organic Light-Emitting Diodes with Enhanced Efficiency; P-Type or E-Type Triplet Conversion to Singlet Excitons? *Adv. Mater.* **2013**, *25*, 1455–1459.
- (13) Ai, X.; Evans, E. W.; Dong, S.; Gillett, A. J.; Guo, H.; Chen, Y.; Hele, T. J. H.; Friend, R. H.; Li, F. Efficient Radical-Based Light-Emitting Diodes with Doublet Emission. *Nature* **2018**, *563*, 536–540.
- (14) Obolda, A.; Zhang, M.; Li, F. Evolution of Emission Manners of Organic Light-Emitting Diodes: From Emission of Singlet Exciton to Emission of Doublet Exciton. *Chin. Chem. Lett.* **2016**, *27*, 1345–1349.
- (15) Obolda, A.; Ai, X.; Zhang, M.; Li, F. Up to 100% Formation Ratio of Doublet Exciton in Deep-Red Organic Light-Emitting Diodes Based on Neutral Pi-Radical. *ACS Appl. Mater. Interfaces* **2016**, *8*, 35472–35478.
- (16) Wu, Q.; Peng, Q.; Niu, Y.; Gao, X.; Shuai, Z. Theoretical Insights into the Aggregation-Induced Emission by Hydrogen Bonding: A Qm/Mm Study. *J. Phys. Chem. A* **2012**, *116*, 3881–3888.
- (17) Obolda, A.; Peng, Q.; He, C.; Zhang, T.; Ren, J.; Ma, H.; Shuai, Z.; Li, F. Triplet-Polaron-Interaction-Induced Upconversion from Triplet to Singlet: A Possible Way to Obtain Highly Efficient OLEDs. *Adv. Mater.* **2016**, *28*, 4740–4746.
- (18) Niu, Y. L.; Peng, Q.; Deng, C. M.; Gao, X.; Shuai, Z. Theory of Excited State Decays and Optical Spectra: Application to Polyatomic Molecules. *J. Phys. Chem. A* **2010**, *114*, 7817–7831.
- (19) Niu, Y.; Li, W.; Peng, Q.; Geng, H.; Yi, Y.; Wang, L.; Nan, G.; Wang, D.; Shuai, Z. Molecular Materials Property Prediction Package (Momap) 1.0: A Software Package for Predicting the Luminescent Properties and Mobility of Organic Functional Materials. *Mol. Phys.* **2018**, *116*, 1078–1090.
- (20) Meyer, H. D.; et al. Using the Mctdh Wavepacket Propagation Method to Describe Multimode Non-Adiabatic Dynamics. *Int. Rev. Phys. Chem.* **2008**, *27*, 569–606.

- (21) Frisch, M. J.; Trucks, G. W.; Schlegel, H. B.; Scuseria, G. E.; Robb, M. A.; Cheeseman, J. R.; Scalmani, G.; Barone, V.; Mennucci, B.; Petersson, G. A. et al. *Gaussian 09*, revision A.1; Gaussian, Inc.: Wallingford, CT, 2009.
- (22) Dreuw, A.; Headgordon, M. Single-Reference Ab Initio Methods for the Calculation of Excited States of Large Molecules. *Chem. Rev.* **2005**, *105*, 4009–4037.
- (23) Peng, Q.; Yi, Y. P.; Shuai, Z.; Shao, J. Toward Quantitative Prediction of Molecular Fluorescence Quantum Efficiency: Role of Duschinsky Rotation. *J. Am. Chem. Soc.* **2007**, *129*, 9333–9339.
- (24) Bendikov, M.; Duong, H. M.; Starkey, K.; Houk, K.; Carter, E. A.; Wudl, F. Oligoacenes: Theoretical Prediction of Open-Shell Singlet Diradical Ground States. *J. Am. Chem. Soc.* **2004**, *126*, 7416–7417.
- (25) Liu, W.; Xiao, Y. Relativistic Time-Dependent Density Functional Theories. *Chem. Soc. Rev.* **2018**, *47*, 4481–4509.
- (26) Yan, P.; Yuan, X.; Yin, S.; Liu, X.; Xu, H.; Yan, B. Multireference Configuration Interaction Study on the Ground and Excited Electronic States of the Alo⁺ Molecule. *Comput. Theor. Chem.* **2017**, *1117*, 258–265.
- (27) Vacher, M.; Bearpark, M. J.; Robb, M. A. Direct Methods for Non-Adiabatic Dynamics: Connecting the Single-Set Variational Multi-Configuration Gaussian (Vm_{cg}) and Ehrenfest Perspectives. *Theor. Chem. Acc.* **2016**, *135*, No. 187.
- (28) Li, J.; Luo, Y.; Zhang, J. A Theoretical Study on Vibronic Spectra and Photo Conversion Process of Protonated Naphthalenes. *Spectrochim. Acta, Part A* **2018**, *205*, 520–527.
- (29) Li, J.; Tian, G.; Luo, Y.; Cao, Z. Theoretical Studies on the Vibrationally-Resolved Absorption and Fluorescence Spectra of H-Pyrene⁺ and H-Coronene⁺. *Chem. Phys. Lett.* **2015**, *641*, 57–61.
- (30) Wang, X. F.; Zuo, G. F.; Li, Z. F.; Li, H. X. Theoretical Study of the Phosphorescence Spectrum of Tris(2-Phenylpyridine)Iridium Using the Displaced Harmonic Oscillator Model. *Acta Phys.-Chim. Sin.* **2015**, *31*, 1667–1676.
- (31) Wang, J.; Xu, X. D.; Phan, H.; Heng, T. S.; Gopalakrishna, Y. T.; Li, G. W.; Ding, J.; Wu, J. Stable Oxindolyl-Based Analogues of Chichibabinqs and Mgllerqs Hydrocarbons. *Angew. Chem.* **2017**, *129*, 14342–14346.
- (32) Filippenko, V.; Frenette, M.; Scaiano, J. C. Solvent-Independent Antioxidant Activity from Thermally Generated Carbon-Centered Radical Antioxidants. *Org. Lett.* **2009**, *11*, 3634.
- (33) Frenette, M.; Aliaga, C.; Font-Sanchis, E.; Scaiano, J. C. Bond Dissociation Energies for Radical Dimers Derived from Highly Stabilized Carbon-Centered Radicals. *Org. Lett.* **2004**, *6*, 2579–2582.
- (34) Weinhold, F.; Glendening, E. D. Comment on “Natural Bond Orbitals and the Nature of the Hydrogen Bond”. *J. Phys. Chem. A* **2017**, *122*, 724–732.
- (35) Ignaczak, A.; Palecz, B.; Belicapacha, S. Quantum Chemical Study and Isothermal Titration Calorimetry of B-Cyclodextrin Complexes with Mianserin in Aqueous Solution. *Org. Biomol. Chem.* **2017**, *15*, 1209–1216.
- (36) Martin, R. L. Natural Transition Orbitals. *J. Chem. Phys.* **2003**, *118*, 4775–4777.
- (37) Lu, T.; Chen, F. Multiwfn: A Multifunctional Wavefunction Analyzer. *J. Comput. Chem.* **2012**, *33*, 580–592.
- (38) Zhang, K.; Liu, J.; Zhang, Y.; Fan, J.; Wang, C.-K.; Lin, L. Theoretical Study of the Mechanism of Aggregation-Caused Quenching in near-Infrared Thermally Activated Delayed Fluorescence Molecules: Hydrogen-Bond Effect. *J. Phys. Chem. C* **2019**, *123*, 24705–24713.
- (39) Stuchebrukhov, A. A. Tunneling Currents in Long-Distance Electron Transfer Reactions. V. Effective One Electron Approximation. *J. Chem. Phys.* **2003**, *118*, 7898–7906.
- (40) Mauchamp, V.; Jaouen, M.; Schattschneider, P. Core-Hole Effect in the One-Particle Approximation Revisited from Density Functional Theory. *Phys. Rev. B* **2009**, *79*, No. 235106.
- (41) Pettersson, L. G. M.; Siegbahn, P. E. M. The Effect of 3d Shell Back Bonding on the Binding of Chlorine Containing Molecules. *J. Chem. Phys.* **1985**, *83*, 3538–3546.